Q. J. R. Meteorol. Soc. (1998), **000**, pp. 1–999

A simplified squall-line model revisited

By ROBERT G. FOVELL* and PEI-HUA TAN

University of California, Los Angeles, USA

(July, 1999)

SUMMARY

We revisit the parameterized moisture model of Garner and Thorpe and show it does indeed support realistic multicellular behavior when an adequate (and commonly available) amount of instability is present in the initial environment. We also consider the dramatic impact that the simplified model's storms have on their upstream environments, and suggest that this is exaggerated by a fundamental shortcoming in the parameterized moisture framework.

KEYWORDS: Squall-lines Parameterized moisture models Multicell storms

1. INTRODUCTION

The typical mature squall-line's quasi-steady circulation features an ascending "front-to-rear" (FTR) jet overlying a descending "rear-to-front" (RTF) current that carries dry, midtropospheric air from the storm's rear flank (Newton 1966; Houze 1993). Some fraction of the lower tropospheric storm inflow exits the storm's forward side in the upper troposphere; this is variously termed the "overturning updraft" (Thorpe et al. 1982) or the "forward anvil outflow". Most of the mass, however, is usually carried in the FTR airflow, which usually leans rearward ("upshear") with height, allowing precipitation to fall behind the storm's leading edge without restricting the inflow. Hydrometeor evaporation beneath the FTR jet establishes and maintains the subcloud cold air pool which underruns the warm, moist boundary layer air, creating a persistent gust front "forced updraft" that provides the initial lifting for air entering the FTR airflow.

Embedded within the FTR airflow are convective "cells", or "free updrafts", periodically generated pockets of enhanced upward motion and convective activity that can be considered "superposed transience" (Moncrieff 1978). New cells usually become established near the storm's leading edge and exist for about an hour as they move rearward within the FTR jet (e.g., Browning et al. 1976). The storm's survival appears to be dependent on its ability to systematically generate new, short-lived replacement cells. At any instant of time, a vertical cross-section taken normal to the mature squall-line reveals a "family" of cells, each representing a different stage of the life cycle. This is commonly referred to as "multicellular" structure and behavior.

Fovell and Tan (1998; hereafter FT) recently presented a detailed analysis of the mature multicellular storm with emphasis on the forcing mechanisms involved in the generation, propagation,and dissipation of its constituent convective cells. They showed that the typical new cell first appears within the the cold pool's forced updraft and quickly becomes positively buoyant. The buoyancy induces a local circulation that, at first, serves to intensify the cold pool forced updraft, aiding the new cell's intensification. However, once the cell begins moving rearward within the FTR flow, the buoyancy-induced circulation starts actively suppressing the forced lifting, even as it forces the entrainment of potentially cold air (from the cold pool and/or the middle troposphere ahead of the storm) into the cell. This entrainment causes the lower portion of the growing cell to become convectively stable while destabilizing the forced updraft farther below.

* Corresponding author: Department of Atmospheric Sciences, University of California, Los Angeles, Los Angeles, CA 90095-1565 USA.

The growing cell thereby becomes "cut off" from the forced updraft, and continues propagating rearward within the FTR airflow. It was concluded that the cellular transience was a direct result of the convectively-generated, buoyancy-induced circulation.

To further our understanding of the cut off and cell regeneration processes, we attempted to identify the simplest dynamical framework capable of capturing this behavior. First, the model was made two-dimensional, as it has been demonstrated that multicellular behavior can be dynamically similar in the two- and three-dimensional frameworks (e.g., Rotunno et al. 1988; FT). Next, condensate loading was deactivated and the complex subgrid turbulence parameterization was replaced by a simple eddy diffusion intended primarily to restrain computational instability. These were found to have little dynamical effect other than to permit the cells to become somewhat stronger and longer-lived. The explicit appearance of precipitation and its attendant timescales were obviated by the adoption of a maintained, lower tropospheric heat sink. Testing revealed that the sink's artificially generated cold pool permitted realistic, long-lived multicellular storms to form with relatively little sensitivity attached to the cooling rate employed.

Finally, the chief role of water vapor is to release latent heat to the surrounding air upon condensing. As the dominant (but not sole) condensation production mechanism is lifting, very simplified models (e.g., Moncrieff and Green 1972; Garner and Thorpe 1992; Jiang and Raymond 1995) have parameterized moisture by making condensation warming proportional to ascent velocity. (The "QCLH" field shown in FT's Fig. 9e lends justification to this approach.) In particular, Garner and Thorpe (1992; hereafter GT) employed this parameterization in a study that explored the role of the vertical wind shear in organizing a squall-line type storm.

GT's mature, upshear-tilted storms apparently assumed one of only two forms, termed herein the "successful" and "unsuccessful" states. The former were virtually steady-state cases marked by the presence of a single free updraft that remained stationary relative to the storm's leading edge. In contrast, the unsuccessful cases possessed but a single, rearward propagating cell updraft that was never replaced by another cell as it moved away from the frontal lifting. The *multicellular* storms that logically should have resided in between these two extreme states were ostensibly missing, a result that stands in very clear contrast to those from more physically sophisticated models in which multicellular behavior is ubiquitous and steady cases are rare. Previous work (e.g., Fovell and Ogura 1989) showed that nearly steady, yet upshear-tilted, storms could be obtained in conditions of intense low-level shear, but not otherwise. Unsuccessful cases are also uncommon if the sounding is sufficiently favorable.

Indeed, GT specifically chose the parameterized moisture framework in order to suppress cell decay and regeneration so that the underlying quasi-steady state may be more clearly revealed. By eliminating microphysical and precipitation timescales, they sought to remove "the main cause of cell decay, i.e., explicit downdraughts of rain-cooled and rain-loaded air". A laudable goal, but was the absence of cellular transience really due to the elimination of explicit moisture from the model? We were motivated to re-examine GT's model framework, to see if the parameterized moisture model was indeed too simple to support multicellular transience.

GT also reported that their successful mature storms exerted a profound and permanent influence on their upstream environments that seems exaggerated when compared to simulations made with more sophisticated models. These storms also developed considerable warming in their overturning updrafts (see their Fig. 7b), at least compared to the buoyancy of their convective updrafts. These results had to be examined closely to see if they were responsible for their model's apparent inability to support multicellular

storms.

Our study is not concerned with GT's ideas regarding the organizing role of shear. Instead, it is an evaluation of the realism and performance of the parameterized moisture framework. That framework, and its implementation, is reviewed in Section 2. Section 3 presents results employing GT's sounding, but focuses specifically on the transition zone between the successful and unsuccessful cases. In Section 4, a more convectively favorable sounding is used. Section 5 presents the conclusions.

2. Model

(a) *The parameterized moisture framework*

In the parameterized moisture (PM) model, the equations concerning moisture are eliminated and the prognostic equation for potential temperature (θ) is rewritten (neglecting mixing) as:

$$\frac{d\theta}{dt} = \beta Q_+ + Q_-, \tag{1}$$

where Q_+ and Q_- are the heating/cooling rates due to vapor condensation warming and liquid water evaporation, and the value of β is conditioned on the sign of the vertical velocity, w:

$$\beta = \begin{cases} 1 & w > 0; \\ 0 & otherwise. \end{cases}$$

The diabatic cooling term, Q_-, is responsible for generating and maintaining the subcloud cold pool. Similar to GT, a shallow, lower tropospheric heat sink of finite size will be used to continually relax the air therein to a preset potential temperature perturbation relative to the initial state, θ_c', with a relaxation time of τ_c.

Following GT, condensational heating is made proportional to updraft velocity, a procedure also adopted by Moncrieff and Green (1972). This is justified in the following manner. The condensational heating term may be written as:

$$Q_+ = \frac{L_v}{c_p \bar{\pi}} \frac{dq_{vs}}{dt} = \frac{L_v}{c_p \bar{\pi}} \frac{dq_{vs}}{dz} \frac{dz}{dt} = w \frac{d\theta_p}{dz}, \tag{2}$$

where L_v is the latent heat of vaporization, c_p is the specific heat of air at constant pressure, $\bar{\pi}$ is the base state nondimensional pressure (a function of height), and q_{vs} is the saturation mixing ratio*. The first equivalence on the right-hand side (RHS) of (2) illustrates that condensational heating results from the temporal change of q_{vs} along a saturated parcel's path. The remaining equivalences presume the relevant motion is primarily upward and follows a moist adiabat. θ_p is the parcel's potential temperature; its vertical gradient describes a moist adiabat in temperature-height space. GT took the moist adiabatic profile to be a simple, specified function of height (see below). The region in which $\frac{d\theta_p}{dz} > 0$ will be termed the unstable layer.

By inserting (2) into (1) and rearranging, physical insight into the PM model's operation is derived. This yields:

$$\frac{\partial \theta}{\partial t} = -u \frac{\partial \theta}{\partial x} - w \left[\frac{\partial \theta}{\partial z} - \beta \frac{d\theta_p}{dz} \right] + Q_-. \tag{3}$$

* It should be noted that this equation incorporates simplifications justified by Wilhelmson and Ogura (1972).

Written in this fashion, it is seen that this term is the PM model's equivalent to FT's "TVPT" term [their equation (2)]. If the grid-scale vertical lapse rate in the unstable layer is smaller than the moist adiabatic value, upward motion will locally increase θ. However, if the lapse rate exceeds the moist adiabatic value, local cooling results even though the parcel is presumed saturated. Note all descent is subsaturated. FT's analysis suggests these are reasonable assumptions, at least in the cloud-bearing layer (see the "TVPT" and "QCLH" fields shown in their Fig. 9). In the usual situation, in which the local potential temperature lapse rate is less than the moist adiabatic value, *both ascent and descent generate warming in the unstable layer.* In this situation, there is no gravity wave activity.

(*b*) *Model implementation*

Our PM model is based on Fovell and Ogura's (1988) anelastic cloud model. Gentle horizontal grid stretching embeds a wide (315 km) high resolution (1 km horizontal grid spacing) region in a very wide ($\approx$1500 km) domain in order to minimize the effects of the open lateral boundaries on the interior solution. The 21 km deep domain's extensive stratospheric layer helps insulate the convective circulation from the unrealistically rigid model top. Vertical grid stretching concentrates the highest resolution in the lower troposphere. The vertical grid spacing is 200 m near the surface and 800 m near the model top. The upper and lower boundaries are both free-slip.

GT presented their results in a nondimensional framework with distances related to the domain depth H. To facilitate comparison, we dimensionalize their results. However, in light of our domain's vertical extent, and the insensitivity of the results to its specific choice, it is more reasonable to relate GT's H to the characteristic depth scale of the model's convective circulation. This will be taken to be 10 km, a physically realistic value for midlatitude storms. Using this figure as a guide, their model's horizontal and vertical grid spacings (roughly 833 and 300 m, respectively) are comparable to ours though their model domain was both shallower (10 km) and narrower (90 km).

The dynamical framework of our PM model differs from GT's in two additional ways (illustrated in Figure 1). First, we elected to make our subcloud heat sink *storm-adaptive* rather than fixed in space. As GT realized, a spatially fixed sink can cause physically inconsistent results if the sink-relative winds are excessively weak or strong. In the former case, the gust front can push upstream from the cooling zone, making the pool shallow and thus incapable of accomplishing much lifting. In the latter situation, the gust front retreats into the cooling zone, causing the storm inflow to be unrealistically cooled before reaching the forced updraft.

In our model, we reconsider the physical position of the cooling zone each time step to keep it properly aligned with the gust front. This technique was tested in the traditional cloud model (with precipitation deactivated) and found to work very well. For greater realism, the cooling zone edge is kept a small distance δ (taken to be 5 km herein) behind the gust front (see Fig. 1) because observations and previous modeling work show that the cooling usually occurs somewhat behind the leading edge. The simulations did not appear to be sensitive to the precise specification of δ, however.

Second, while GT's unstable region spanned the entire domain width, the forward extent of ours is truncated, extending no farther than a small distance ϵ (fixed at 5 km herein) ahead of the surface gust front position (see Fig. 1). Since all rising parcels in the unstable region are presumed saturated, whatever their origin, we perceived the need to differentiate middle tropospheric parcels within the FTR airflow (which likely originated in the low-level storm inflow and thus would be saturated) from those residing in the environment farther ahead (which would not likely have been displaced far enough

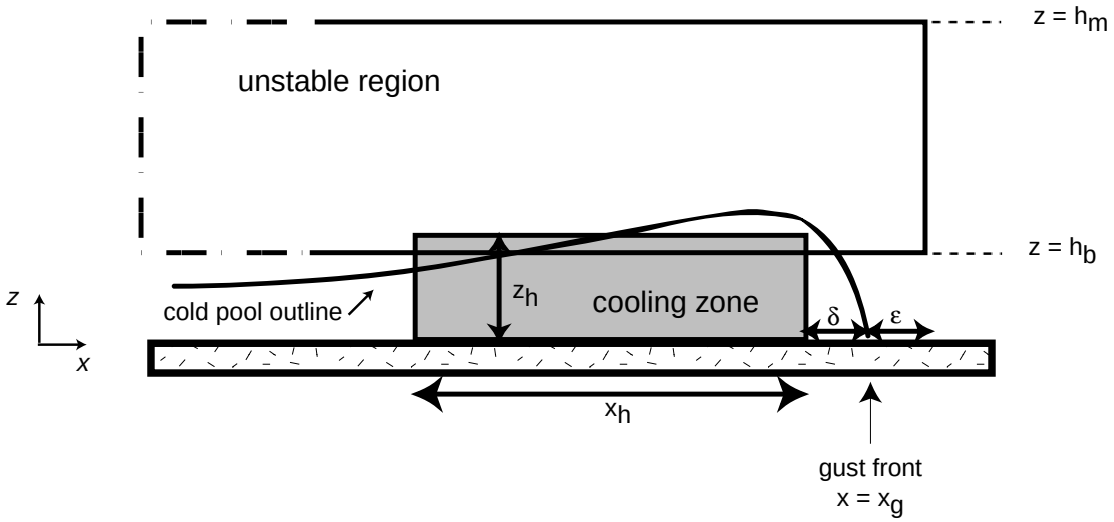

Figure 1. Schematic diagram for the parameterized moisture model. The unstable region extends laterally rearward to the domain's west boundary. See text.

vertically to become saturated). By truncating the unstable region, the environment ahead of the storm is permitted to adjust to the presence of convection through transient gravity wave activity.

It should be noted that this truncation disallows the development of downshear-tilted updrafts but, as noted by GT, such an updraft orientation is inconsistent with the manner in which the evaporational cooling is parameterized anyway. It turned out that the results were not especially sensitive to the choice of ϵ, so long as it was not made too small. For reasons to be discussed later, the unstable region's rearward extent is not truncated, although it has been shown (e.g., by FT) that convective cells degenerate into gravity wave disturbances as they propagate towards the storm's rear.

3. Results with GT's sounding

Figure 2 illustrates GT's initial sounding and handling of the moist adiabatic lapse rate, dimensionalized presuming H = 10 km. A 3 K temperature excess could be realized at 7 km ($z = h_m$) for a parcel raised undiluted from the undisturbed lower troposphere. "Cloud base" and the level of free convection coincide at 1 km ($z = h_b$), while "cloud top" is expected at 9 km ($z = h_t$).

The cooling zone was prescribed to be z_h = 1.5 km deep and x_h = 45 km wide, with thermal perturbation θ'_c = -4.5 K. For each case, the storm speed is the domain translation rate that kept the cooling zone and gust front stationary relative to the grid during maturity. We found using a wide cooling zone helped minimize sensitivity to domain translation. In a few (notably the most weakly sheared) cases, however, no single translation speed kept the mature phase cold pool stationary; the pool always moved more slowly than the domain. The relaxation time τ_c of 600 sec was adopted; no sensitivity to this parameter was discovered.

Table 1 summarizes a set of simulations in which the shear intensity was varied from 3 x 10^{-3} to 4 x 10^{-3} s^{-1} for a constant shear layer confined to the lowest 3

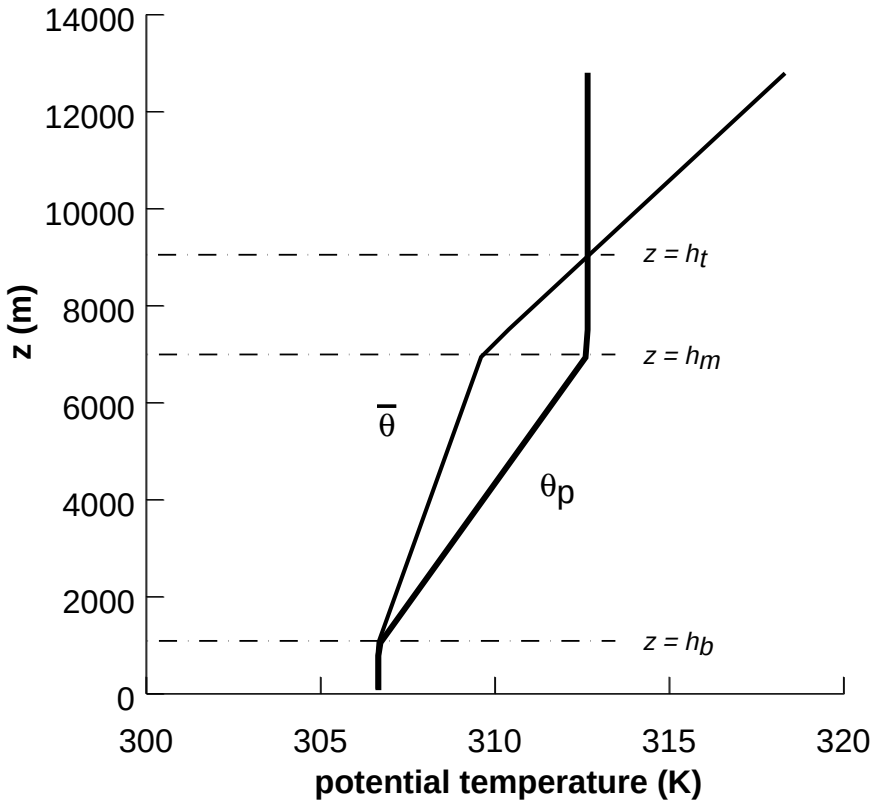

Figure 2. GT's sounding. $\bar{\theta}$ is the potential temperature of the initial environmental state, while θ_p represents the path taken by a saturated parcel rising from the undisturbed lower troposphere.

km. This experiment includes the transition from unsuccessful to successful states that GT analyzed and involves shear parameters comparable to those examined with more physically sophisticated cloud models by Fovell and Ogura (1989) and Fovell and Dailey (1995). It should be noted that we are not attempting to recreate GT's entire experiment.

TABLE 1. Mature phase storm statistics for simulations with the GT sounding.

Shear intensity (10^{-3} s^{-1})	Storm speed (m s^{-1})	Storm behavior	Bulk Richardson number
3.0	unobtainable	not applicable	27
3.1	10.2	steady unsuccessful	25
3.15	11.5	unsteady multicell	24
3.25	11.6	unsteady multicell	23
3.5	12.5	nearly steady unicell	20
4.0	13.2	steady unicell	15

Despite physical and numerical differences, we were able to replicate GT's results to a fairly high degree. As in GT, the smaller (larger) shear intensities resulted in nearly

steady unsuccessful (successful) cases. An example of a nearly steady unsuccessful case, resulting from a shear intensity of 3.1 x 10^{-3} s^{-1}, is shown in Fig. 3a*. One deep free updraft maintained by parameterized condensation warming was produced early on, but the storm remained devoid of any deep convective activity after it was swept rearward. Figure 3b shows a nearly steady successful (or unicell) case made with a 3.5 x 10^{-3} s^{-1} shear intensity. An extremely small amount of transience, with a period of roughly 28 min, was superposed upon its deep upshear-tilted updraft (see Fig. 4.7 of Tan 1997) without changing its fundamental shape or position. This behavior is reminiscent of Fovell and Ogura's (1989) most strongly sheared case, which possessed considerably larger shear (12 x 10^{-3} s^{-1}) over a somewhat shallower depth (2.5 km).

In our PM model, *multicellular storms do indeed exist.* However, their appearance is restricted to a very narrow region within the parameter space. The balance of Fig. 3 shows how the 3.15 x 10^{-3} s^{-1} case behaved over a typical 24 min period during its mature phase. In Fig. 3c, a nearly discrete updraft (cell) may be seen above $x = 28$ km, just rearward of a deep updraft extending upwards from the forced updraft zone at the gust front. This cell was in the process of separating from the deep updraft at the time shown, and continued propagating rearward within the FTR flow as time progressed. As it moved away, the forced lifting began redeveloping upward [panels (d) and (e)], establishing a new, discrete maximum in warming (positive potential temperature perturbation) within it. The upper portion of this reinvigorated updraft eventually separated [panel (d)], and this cell closely mimicked the behavior of its predecessor. The cell period in this case was again about 28 min.

Though clearly multicellular, this case closely resembles Fovell and Ogura's (1989) "weakly evolving" storm (their Fig. 16), which possessed 9 x 10^{-3} s^{-1} of shear in the lowest 2.5 km. The main point is that the elimination of microphysical time scales, water loading and rain-cooled downdrafts was not sufficient to eradicate this oscillatory behavior. Though they weaken, these cells never degenerate into gravity waves as they propagate through the storm's trailing region as usually occurs in more sophisticated models, but this is because the cells never become starved of "water vapor" (see next section). As they propagate through the unstable region, their updrafts continue to generate parameterized condensation warming, even when they are far removed from the moisture source at the storm's leading edge, and naturally there is no water loading to assist in weakening the drafts. None of these factors turned out to be necessary conditions for supporting temporal unsteadiness, and their elimination did not preclude the development of such behavior.

4. Results with a more realistic sounding

(*a*) *Multicellular behavior and new cell generation*

Although the PM model has been shown to support (albeit somewhat rudimentary) multicellular behavior, it remains that the portion of the shear intensity/depth parameter space occupied by such cases was extremely narrow. In addition, even this small multicellular segment could be eliminated by a relatively minor increase in the model's explicit diffusion. Yet, as noted earlier, multicellular unsteadiness is ubiquitous in typical cloud model experiments.

This discrepancy appears to be rooted in the model's initial conditions rather than in its physics. While GT considered very realistic values of shear intensity and layer

* This was the weakest shear case that proved to be independent of the domain translation speed (see Table 1).

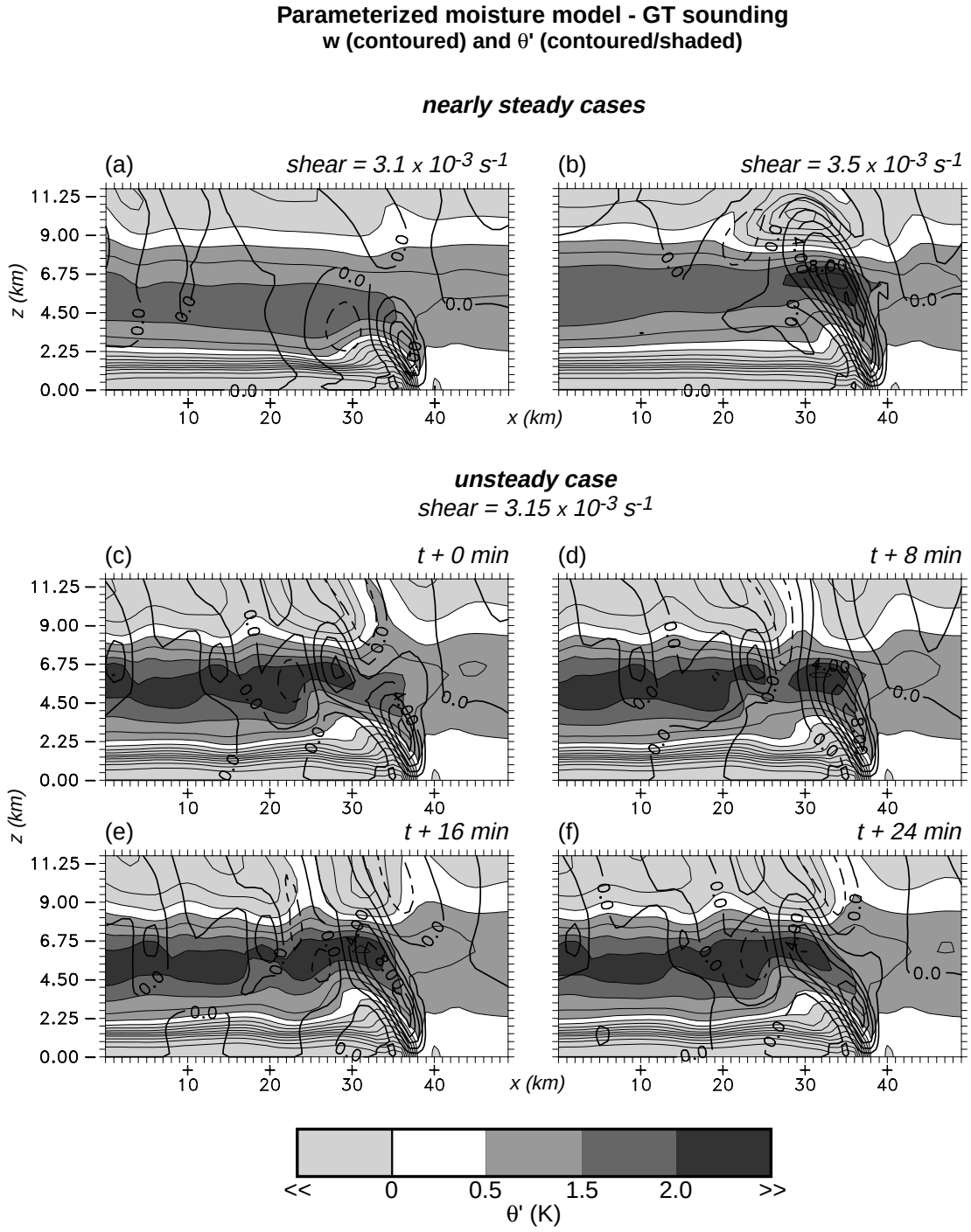

Figure 3. Instantaneous mature phase fields of vertical velocity (w; 2 m s^{-1} contours) and perturbation potential temperature relative to the intitial state (θ'; shaded with 0.5 K contours) for three parameterized moisture simulations made with GT's sounding. In each case, only a portion of the domain is shown, and horizontal axes are labeled relative to the left side of the subdomain depicted. Negative w contours are dashed.

depth, their sounding (Fig. 2) possessed only about 400 J kg^{-1} of convective available potential energy (CAPE), far less than the average value of 2260 J kg^{-1} found for severe midlatitude squall-line environments by Bluestein and Jain (1985). Moncrieff and Green (1972) were among the first to suggest that a ratio formed from the CAPE and a function of the vertical shear, representing a nondimensional bulk Richardson number (BRi), can be skillful in delineating among storm types and modes of convection. Weisman and Klemp's (1982) three-dimensional simulations showed BRi values between 30 and 400 resulted in multicellular storms, while supercells were commonly found for BRi $<$ 30. Because the CAPE of GT's sounding was very small, so too were the BRi values within their parameter space (Table 1), being mainly in the Weisman-Klemp supercell range*.

The more realistic "FO-MOD" profile shown in Fig. 4 originated with the moderate (2500 J kg^{-1}) CAPE "FO" sounding used in Fovell and Ogura (1988) and Fovell and Tan (1998), among others. As crude yet simple compensation for the PM model's lack of water loading the undiluted parcel temperature excess was uniformly discounted by 25% between the LFC and equilibrium levels; this reduced the CAPE to 1800 J kg^{-1}. We examined shear intensities in the range 3 x 10^{-3} to 6 x 10^{-3} s^{-1}, again given a 3 km shear layer depth (see Table 2). Note that this experiment samples a much more realistic range of BRi values. These simulations also employed a more realistic cold pool cooling of θ_c' = -10 K within a deeper (z_h = 2 km) cooling zone. The latter was necessitated by the fact that with a more unstable sounding, the cold pool tended to be shallower, even when stronger cooling was enforced within the cooling zone.

TABLE 2. Mature phase storm statistics for simulations with the FO-MOD sounding.

Shear intensity (10^{-3} s^{-1})	Storm speed (m s^{-1})	Storm behavior	Bulk Richardson number
3.0	unobtainable	not applicable	123
3.2	10.4	steady unsuccessful	108
3.25	12.6	unsteady multicell	105
3.5	13.5	unsteady multicell	91
3.7	13.6	unsteady multicell	81
3.8	13.7	unsteady multicell	77
4.0	14.1	unsteady multicell	69
4.25	14.5	unsteady multicell	61
4.5	15.5	unsteady multicell	55
5.0	16.1	unsteady multicell	44
6.0	18.1	steady unicell	31

It may be noted in Table 2 that steady unsuccessful and unicellular storms were still obtained, but in between the parameter space occupied by unsteady multicellular storms was much larger*. One specific case, having a shear intensity of 4 x 10^{-3} s^{-1}, is presented in Fig. 5. This storm generated new cells at roughly 10 min intervals, so the figure spans slightly more than one cell generation cycle. In panel (a), the forced updraft above x = 38 km was in the process of spawning a new convective cell ahead of the older cell located above x = 30 km. The new cell subsequently developed rapidly while translating

* Computation of BRi values followed Bluestein and Jain (1985).

* Again, we could not obtain a translation-insensitive simulation for the 3 x 10^{-3} s^{-1} case. This did not occur in the more physically realistic cloud model when a similar buoyancy sink was employed, and may be a limitation related to the moisture parameterization.

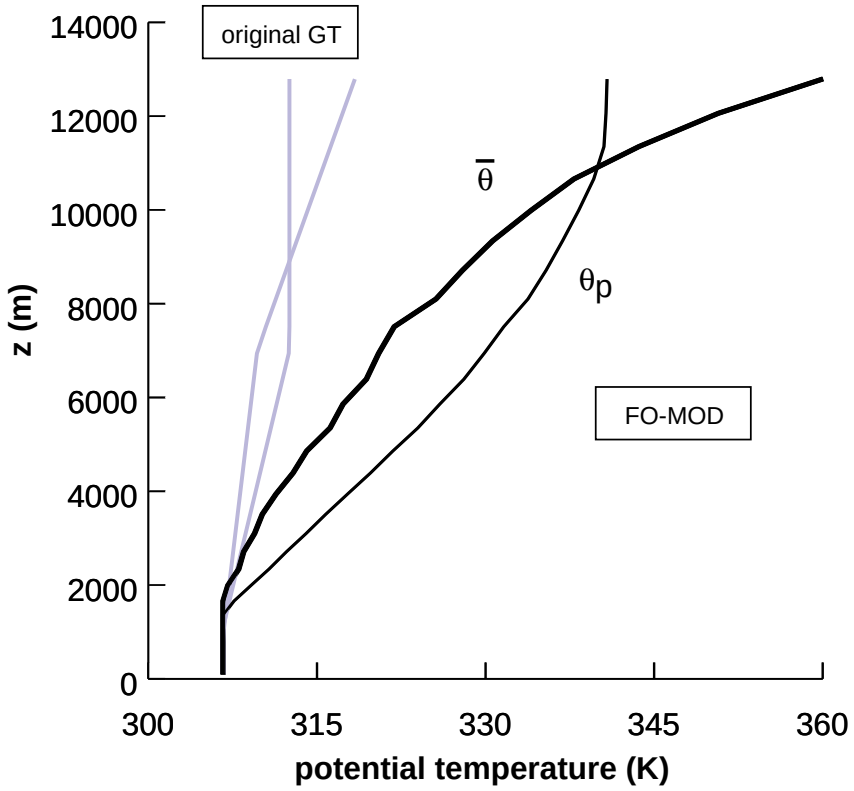

Figure 4. As in Fig. 2, but for the FO-MOD sounding. GT's sounding is shown for reference.

rearward [panel (b)] and reached maximum intensity around the time shown in panel (c). At that time, the cell was already becoming cut off from the low-level forced lifting, and the development of the next convective cell commenced shortly thereafter [panel (d)]. The basic sequence of events is dynamically similar to that seen in the GT sounding simulation (Fig. 3), though in the present case the convective cells are more discrete as well as considerably more intense (with maximum updraft intensities exceeding 20 m s^{-1}), the latter reflecting the FO-MOD sounding's greater instability.

The multicellular behavior displayed in this case also compares favorably to that described by FT, despite the many simplifications inherent in removing explicit moisture. Figure 6 shows how the buoyancy contribution to the vertical velocity acceleration (given by $g\theta'\bar{\theta}^{-1}$) varied locally over the two minute period prior to each time shown. Parameterized condensation warming caused the substantial increase in upward buoyancy acceleration at the developing cell's top (above $x = 38$ km at $z = 4$ km) in Fig. 6a. This positive buoyancy, however, induced a local circulation that over the next several minutes not only served to further the developing cell's ascent but also caused the entrainment of less buoyant air into the cell beneath its center (where the updraft is most intense). The latter is manifested by the local decrease in both the buoyancy perturbation (compare Figs. 5a and b) and the upward buoyancy acceleration (Fig. 6b) that occurred at and below the cell center around $x = 34$ km during the preceding several minutes. Passive

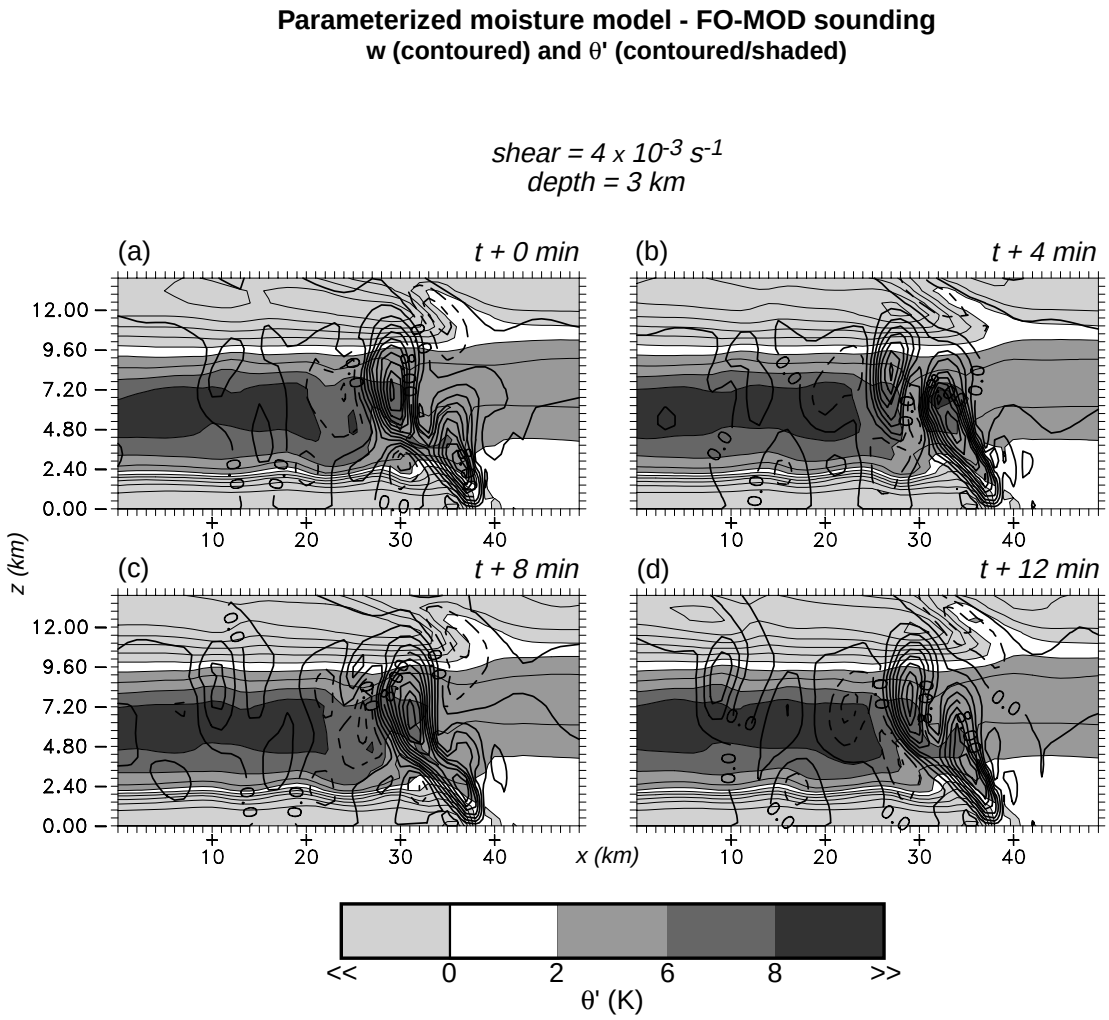

Figure 5. As in Fig. 3, but for a simulation made using the FO-MOD sounding. The θ' contour interval is 2 K.

tracer analysis (not shown) revealed that, as in FT, the entrained air was drawn both from the negatively buoyant cold pool beneath the growing cell as well as from the nearly neutrally buoyant air residing in the storm's midlevel inflow. The sense of the buoyancy-induced entrainment is indicated qualitatively on the Fig. 6b by the white arrows.

As discussed in FT, the entrainment convectively stabilized the growing cell's lower portion, eventually causing the cell to both weaken and become cut off from the forced updraft. Simultaneously, it redestabilized the upper portion of the forced updraft (above x = 36 km in Fig. 6c), ultimately culminating in the development of yet another convective cell (Fig. 6d). The cut off process was dependent upon the cell updraft generating sufficient warming to drive the entrainment, and this was facilitated by the FO-MOD sounding's greater CAPE. Thus, it is concluded that the underlying physics of the oscillatory temporal behavior can be adequately, if crudely, captured in this very simplified

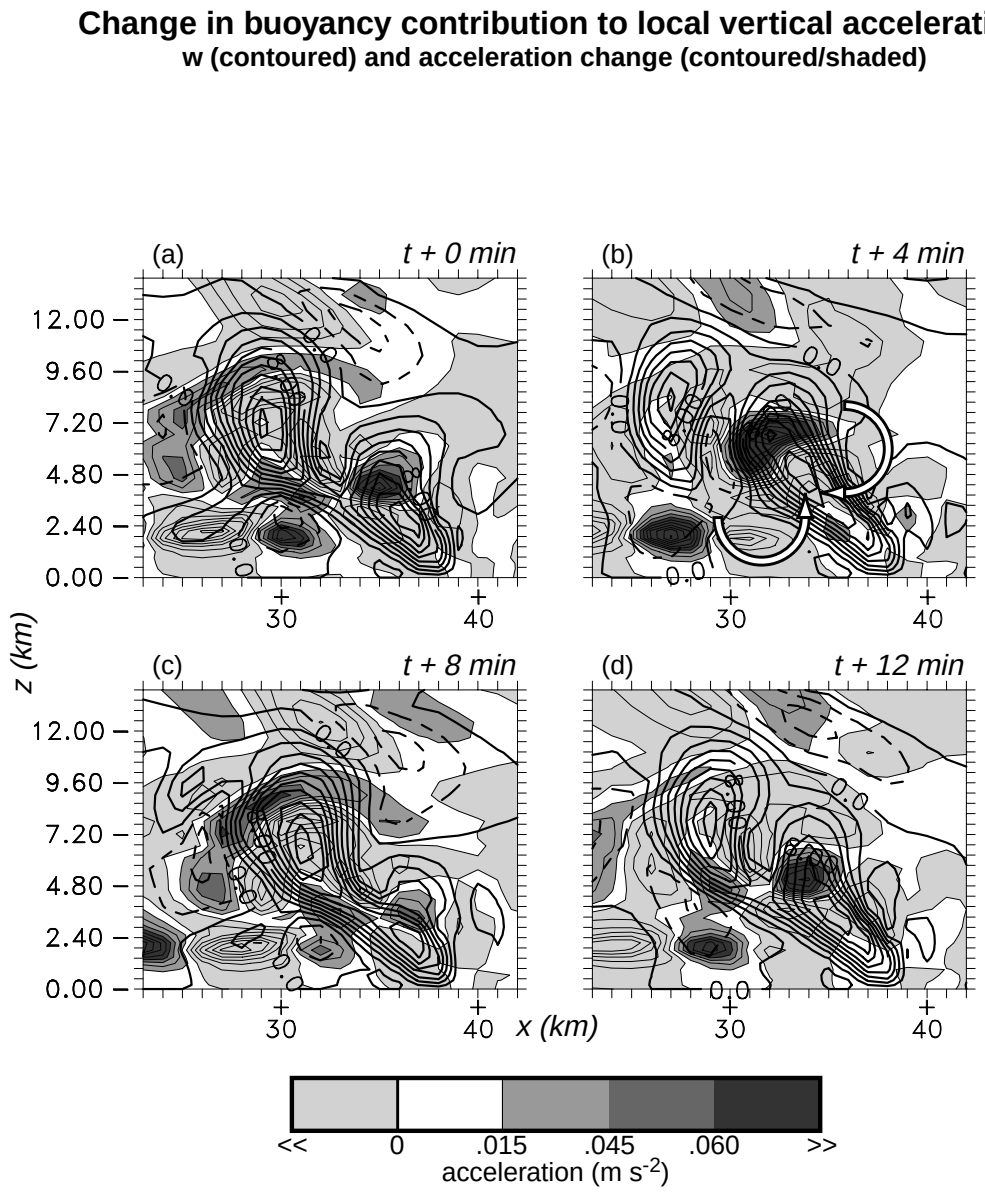

Figure 6. Change in the buoyancy contribution to the local vertical velocity acceleration (shaded with .015 m s^{-1} contours) over the two minute period prior to each time shown (see text), superimposed with vertical velocity (2 m s^{-1} contours), for comparison with Fig. 5. Subdomain axes labeled relative to that shown in Fig. 5. Negative w contours are dashed.

model.

A further similarity between the PM and more physically sophisticated cloud models appears in the manner in which new convective cells are triggered. FT found that a new development was often preceded by the appearance of a "daughter cloud", formed as a consequence of the previous cell's buoyancy-induced circulation, just ahead (upstream)

of the gust front (see their Figs. 3, 15 and 16). Rapid reintensification of the forced lifting occurred as the storm inflow carried the daughter cloud's updraft over the gust front. A similar phenomenon is seen in the PM model storms. In Fig. 5b, the daughter cloud updraft resides above $x = 40$ km, ahead of the gust front but still within the truncated unstable zone, at about $z = 2.5$ km. Four minutes later (Fig. 5c), the updraft's position is directly above the forced updraft, which had markedly weakened over the preceding several minutes. Rapid reintensification of the forced updraft follows immediately, leading to the new cell shown in Fig. 5d. A more comprehensive examination is presented in Tan (1997).

(*b*) *Upstream modification*

As noted previously, GT's model storms exerted considerable influence on their upstream environments in the form of significant upper tropospheric warming, a very strong forward anvil outflow and substantially enhanced lower tropospheric inflow. The latter two, which are related through mass continuity (Fovell and Ogura 1988), combined to radically alter the tropospheric vertical wind shear from its original configuration, a point which GT emphasized. Our PM simulations with the GT sounding were qualitatively similar to GT's results in these respects, and the adoption of the more realistic FO-MOD sounding aggravated the upstream modification even further.

These modifications seem excessive when compared to results from more physically realistic models. Figures 3 and 5 clearly show that restricting the unstable region's horizontal extent did not discourage the accumulation of upper tropospheric warming in the upstream environment. Passive tracer analysis (not shown) confirmed that this warming was generated in the convective updrafts and subsequently advected into the upstream environment in the storm's intense forward anvil outflow. The strength of the outflow in this case can be judged from Fig. 7, which shows an instantaneous vertical profile of the ground-relative horizontal wind taken at a location 20 km upstream (east) of the surface gust front position (black dotted line), along with the initial profile*. Note also the considerably enhanced westward flow in the lower troposphere, leading to a somewhat different, but still profound, alteration of the tropospheric vertical shear than that found by GT (see their Fig. 8).

For comparison, Fig. 7 also shows instantaneous mature phase wind profiles taken from two traditional cloud model simulations made using the same initial wind profile and with the FO sounding. One simulation employed the anelastic model with precipitation deactivated and fitted with a storm-adaptive cold pool. The other was made with a compressible model with full warm rain microphysics in which convection was initiated with a positively buoyant thermal. In both cases, the upstream profiles are far less disturbed, especially in the lower troposphere.

Analysis suggests the dramatic upstream influence in the PM simulations is due to a fundamental shortcoming of the parameterized moisture framework. In reality, as convective cells traverse rearward, the amount of vapor within them is depleted as they move away from the vapor's low-level source. Thus, the updrafts progressively generate less warming, which in turn causes the updrafts themselves to weaken until they degenerate into convectively inactive gravity waves. In the PM model, however, parameterized latent heat release is proportional to the updraft velocity. As long as the updraft persists, it can generate the warming needed to maintain the rising motion. As a result, these cells never really "die" or lapse into stable gravity waves as they propagate

* The storm-relative winds were obtained by subtracting the ground-relative storm speed.

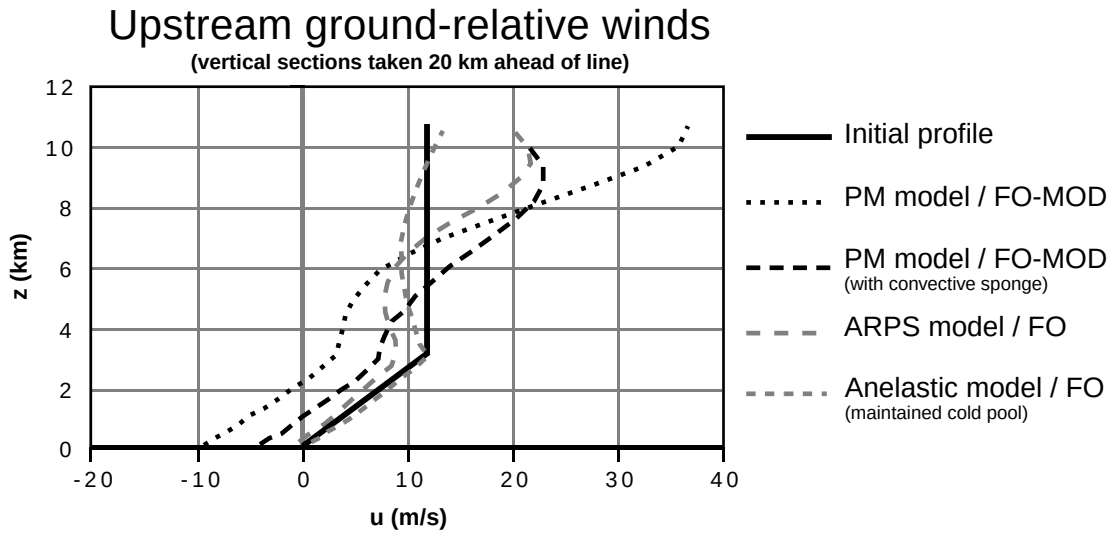

Figure 7. Instantaneous mature phase vertical profiles of ground-relative horizontal wind, taken at a location 20 km upstream of the surface gust front position. The parameterized moisture (PM) simulations utilized the FO-MOD sounding. The other runs used the original FO sounding. All simulations employed the same initial wind profile shown.

rearward, but instead remain convectively active and continue (along with subsidence) to generate warming which accumulates downstream of the storm's leading edge.

Figure 8 shows some additional instantaneous fields for this simulation, for the same time presented in Fig. 5a. The accumulated warming on the storm's rear side [panel (a)] results in the establishment of high perturbation pressure in the upper troposphere there [panel (d)]*. The resulting horizontal pressure gradient drives the unrealistically strong forward anvil outflow [panel (c)] which, owing to mass continuity, is compensated by significantly enhanced lower tropospheric inflow in the upstream environment. The advection of positively buoyant air into the upstream environment by the forward anvil outflow actually serves to reduce the horizontal pressure gradient by establishing (weaker) high perturbation pressure in the upper troposphere ahead of the storm as well. In one test, the upstream upper tropospheric warming was reduced by locally introducing Newtonian cooling there (i.e., for $x > 35$ km) during the mature phase. That had the effect of *intensifying* the forward anvil outflow (and enhancing the low-level inflow) even more owing to the increased horizontal pressure gradient.

We initially attempted to address this shortcoming by limiting the rearward extent of the unstable region. This failed because the cells translated rearward only to the western edge of this region, where they effectively became stationary†. This made the results profoundly sensitive to the specified unstable region width. We tried to fashion a passive tracer (mimicking equivalent potential temperature) and relate condensational warming not only to the magnitude of the lifting but also to the tracer concentration. This also did not work well, and in fact made the model about as complicated as the

* A constant may be added or subtracted from the perturbation pressure field, as the model requires only pressure gradients.

† Actually, the cells continuously redeveloped just inside of the unstable zone.

typical cloud model, violating the spirit of the simplification.

As a very crude way of treating the problem, and merely to support our explanation for the source of the upstream modification, we implemented (through Newtonian cooling) a "convective sponge" in the unstable region. The sponge was applied only to positive potential temperature perturbations and relaxed those perturbations to zero over a certain time period. The convective sponge time scale chosen (10 min) was long relative to the rate of heat release in the principal updrafts (active cells) but shorter than the time necessary for those drafts to propagate rearward, and thus the sponge crudely forced the weakening in convective heating usually noted as cells translate and age.

Figure 8 also shows instantaneous fields for the convective sponge simulation, at a time chosen to enhance the comparison with the original run. The active cells in the convective sponge run were little affected (compare panels [b] and [f]), but the amount of accumulated downstream warming was dramatically reduced (panels [a] and [e]). Consequently, the perturbation pressure excess in this region was smaller (panels [d] and [h]), leading to a substantially weaker forward anvil outflow in the upper troposphere ahead of the storm (panels [c] and [g]). The upstream region vertical profile of the horizontal wind for this case is also shown in Fig. 7 (marked by the long black dashed line). Though discrepancies remain, the degree of upstream modification more closely resembles the results from the traditional cloud models. Unlike the original simulation, much of the present storm's inflow was carried rearward in the FTR jet rather than overturned into the forward anvil outflow. This resulted in the establishment of a strong RTF current, and an more realistic-looking circulation overall.

5. Summary and conclusions

Garner and Thorpe (1992; "GT") employed a parameterized moisture (PM) model to elucidate the role of vertical wind shear in organizing squall-line storms. During maturity, a typical storm possesses a large-scale background circulation in which sequentially generated, short-lived convective cells are embedded. GT chose the simplified model because, in their view, it inherently "suppressed cell decay and redevelopment", permitting them to focus on the much steadier background circulation. Indeed, their model yielded "extraordinarily steady" solutions that were either successful (consisting of a single, persistent deep updraft) or unsuccessful (devoid of deep convection) during maturity. "Multicellular" storms were ostensibly absent.

Based on Fovell and Tan's (1988) analysis, however, we suspected the PM model should support cell redevelopment. Our examination showed that GT's initial environment lacked sufficient convective instability to drive the episodic entrainment process critical to cellular transience. Given a commonly available amount of instability, even the PM model was found to support realistic-looking multicellular storms. Steady unsuccessful and successful storms still existed, but in between, the parameter space region occupied by multicell storms was substantially larger.

Less realistic was the degree to which PM model storms influenced their upstream environments. Analysis suggested the exaggerated impact could be traced to a fundamental shortcoming of the simplified model: that convective cells, once formed, did not dissipate, even as they propagated far away from the storm's leading edge. This permitted an excess of parameterized condensation warming to build up in the storm's trailing region, with a substantial impact on the storm's overall circulation.

GT's study helped demonstrate that both shear intensity and shear layer depth combine to influence the mature squall-line storm's background, quasi-steady circulation. Indeed, by examining an environment with small convective instability, they showed the

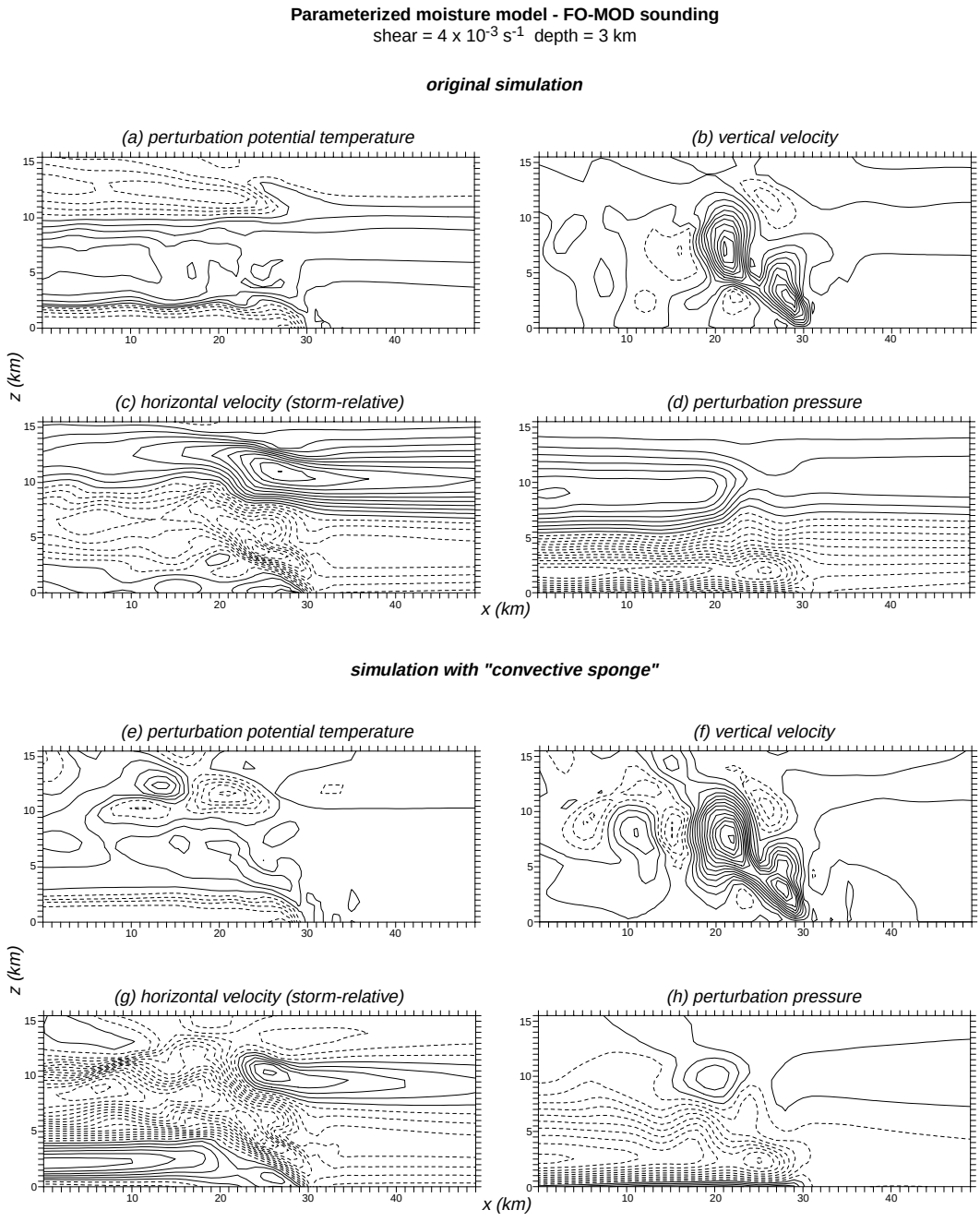

Figure 8. Instantaneous model fields for two parameterized moisture model simulations, without and with a "convective sponge", made using the FO-MOD sounding. (a), (e): perturbation potential temperature (2 K contours); (b), (f): vertical velocity (2 m s^{-1} contours); (c), (g): storm-relative horizontal velocity (3 m s^{-1} contours); (d), (h): perturbation pressure (0.5 mb contours). Storm speeds were 14.1 and 18.8 m s^{-1}, respectively. In each case, only a portion of the domain is shown. Negative contours are dashed.

transition between the successful and unsuccessful cases can be very narrow, thereby emphasizing the contrast between these two extreme states without the distraction posed by multicellular transience. Our contribution is to show that the PM model also supports reasonable multicellular behavior when more realistic environmental conditions are employed. However, our analysis also points to deficiencies in the PM framework that serve to limit its general applicability.

Acknowledgement

This work was supported by the National Science Foundation (NSF) under grant ATM94-21847.

References

Bluestein, H. B. and Jain, M. H. 1985 Formation of mesoscale lines of precipitation: severe squall lines in Oklahoma during the spring. *J. Atmos. Sci.*, **42,** 1711–1732

Browning, K. A., Fankhauser, J. C., Chalon, J.-P., Eccles, P. J., Strauch, R. C., Merrem, F. H., Musil, D. J., May, E. L. and Sand, W. R. 1976 Structure of an evolving hailstorm. Part V: Synthesis and implications for hail growth and hail suppression. *Mon. Wea. Rev.*, **104,** 603–610

Fovell, R. G. and Dailey, P. S. 1995 The temporal behavior of numerically simulated multicell-type storms, Part I: Modes of behavior. *J. Atmos. Sci.*, **52,** 2073–2095

Fovell, R. G. and Ogura, Y. 1988 Numerical simulation of a midlatitude squall line in two dimensions. *J. Atmos. Sci.*, **45,** 3846–3879

1989 Effect of vertical wind shear on numerically simulated multicell storm structure. *J. Atmos. Sci.*, **46,** 3144–3176

Fovell, R. G. and Tan, P.-H. 1998 The temporal behavior of numerically simulated multicell-type storms, Part II: The convective cell life cycle and cell regeneration. *Mon. Wea. Rev.*, **126,** 551–577

Garner, S. T. and Thorpe, A. J. 1992 The development of organized convection in a simplified squall-line model. *Q. J. R. Meteorol. Soc.*, **118,** 101–124

Houze, R. A., Jr. 1993 *Cloud Dynamics.* Academic Press, San Diego. 573 pp.

Jiang, H. and Raymond, D. J. 1995 Simulation of a mature mesoscale convective system using a nonlinear balance model. *J. Atmos. Sci.*, **52,** 161–175

Ludlam, F. H. 1963 Severe local storms: A review. *Severe Local Storms., Meteor. Monog.*, No. 27, Amer. Meteor. Soc., 1–30

Moncrieff, M. W. 1978 The dynamical structure of two-dimensional steady convection in constant vertical shear. *Q. J. R. Meteorol. Soc.*, **104,** 563–567

Moncrieff, M. W. and Green, J. S. A. 1972 The properties and transfer properties of steady convective overturning in shear. *Q. J. R. Meteorol. Soc.*, **98,** 336–352

Rotunno, R., Klemp, J. B. and Weisman, M. L. 1988 A theory for strong, long lived squall lines. *J. Atmos. Sci.*, **45,** 463–485

Tan, P.-H. 1997 *Numerical investigation of the nature of multicellular storms.* Ph. D. thesis, University of California, Los Angeles, 243 pp.

Thorpe, A. J., Miller, M. J. and Moncrieff, M. W. 1982 Two-dimensional convection in non-constant shear: A model of mid-latitude squall lines. *Q. J. R. Meteorol. Soc.*, **108,** 739–762

Weisman, M. L. and Klemp, J. B. 1982 The dependence of numerically simulated convective storms on vertical wind shear and buoyancy. *Mon. Wea. Rev.*, **110,** 504–520

Wilhelmson, R. B. and Ogura, Y. 1972 The pressure perturbation and the numerical modeling of a cloud. *J. Atmos. Sci.*, **29,** 1295–1307

Figure captions

Figure 1 - Schematic diagram for the parameterized moisture model. The unstable region extends laterally rearward to the domain's west boundary. See text.

Figure 2 - GT's sounding. $\bar{\theta}$ is the potential temperature of the initial environmental state, while θ_p represents the path taken by a saturated parcel rising from the undisturbed lower troposphere.

Figure 3 - Instantaneous mature phase fields of vertical velocity (w; 2 m s^{-1} contours) and perturbation potential temperature relative to the intitial state (θ'; shaded with 0.5 K contours) for three parameterized moisture simulations made with GT's sounding. In each case, only a portion of the domain is shown, and horizontal axes are labeled relative to the left side of the subdomain depicted. Negative w contours are dashed.

Figure 4 - As in Fig. 2, but for the FO-MOD sounding. GT's sounding is shown for reference.

Figure 5 - As in Fig. 3, but for a simulation made using the FO-MOD sounding. The θ' contour interval is 2 K.

Figure 6 - Change in the buoyancy contribution to the local vertical velocity acceleration (shaded with .015 m s^{-1} contours) over the two minute period prior to each time shown (see text), superimposed with vertical velocity (2 m s^{-1} contours), for comparison with Fig. 5. Subdomain axes labeled relative to that shown in Fig. 5. Negative w contours are dashed.

Figure 7 - Instantaneous mature phase vertical profiles of ground-relative horizontal wind, taken at a location 20 km upstream of the surface gust front position. The parameterized moisture (PM) simulations utilized the FO-MOD sounding. The other runs used the original FO sounding. All simulations employed the same initial wind profile shown.

Figure 8 - Instantaneous model fields for two parameterized moisture model simulations, without and with a "convective sponge", made using the FO-MOD sounding. (a), (e): perturbation potential temperature (2 K contours); (b), (f): vertical velocity (2 m s^{-1} contours); (c), (g): storm-relative horizontal velocity (3 m s^{-1} contours); (d), (h): perturbation pressure (0.5 mb contours). Storm speeds were 14.1 and 18.8 m s^{-1}, respectively. In each case, only a portion of the domain is shown. Negative contours are dashed.